RAA 2017 Vol. **17** No. **9**, 99 (10pp) doi: 10.1088/1674–4527/17/9/99

http://www.raa-journal.org *http://iopscience.iop.org/raa*

***R**esearch in*
***A**stronomy and*
***A**strophysics*

Research on design of adaptive connecting mechanisms for the cable-net and panels of FAST

Peng Jiang, Qing-Wei Li and Ren-Dong Nan

[1] National Astronomical Observatories, Chinese Academy of Sciences, Beijing 100012, China; *pjiang@nao.cas.cn, qwli@nao.cas.cn, nrd@nao.cas.cn*

[2] Key Laboratory of Radio Astronomy, Beijing 100012, China

Received 2016 November 29; accepted 2017 July 4

Abstract The reflector system of the Five-hundred-meter Aperture Spherical radio Telescope (FAST) is designed to incorporate 4450 rigid panels supported by a flexible cable-net structure. The shape-changing operation that occurs in the process of observation will lead to a relative displacement between adjacent nodes in the cable-net. In addition, three nodes on a rigid panel are fixed with respect to each other. Thus, adaptive connecting mechanisms between panels and the cable-net are certainly needed. The present work focuses on the following aspects. Firstly, the degrees of freedom of adaptive connecting mechanisms were designed so that we can not only adapt the panel to the deformation of the cable-net, but also restrict the panel to its right place. Secondly, finite element and theoretical analyses were applied to calculate the scope of motion in adaptive connecting mechanisms during the cable-net's shape-changing operation, thus providing input parameters for the design size of the adaptive connecting mechanisms. In addition, the gap size between the panels is also investigated to solve the trade-off between avoiding panel collisions and increasing the observation efficiency of FAST.

Key words: telescopes — Astronomical Instrumentation, Methods and Techniques — methods: analytical — methods: data analysis

1 INTRODUCTION

The Five-hundred-meter Aperture Spherical radio Telescope (FAST) is the largest single-aperture radio telescope under construction anywhere in the world. According to the working principle of FAST (illustrated in Fig. 1), the supporting structure of the reflector system should be capable of forming a parabolic surface from a spherical surface (Nan et al. 2003, 2011). This is the most prominent special requirement of the telescope beyond those of conventional structures. By considering the uniformity needed for stress distribution, a cable-net structure was chosen to have the form of a geodesic mesh. The cable-net comprises 6670 steel cables and approximately 2225 cross nodes. The cross nodes of the cable-net are used as control points. Each control point is connected to an actuator by a down-tied cable (Li et al. 2001; Luo et al. 2000, 2003; Ren et al. 2001; Lu & Ren 2007). By controlling the actuator using feedback from the measurement and control system, the positions of the cross nodes can be adjusted to form an illuminated aperture having a diameter up to 300 m. This illuminated aperture moves along the spherical surface according to the zenith angle of the target objects (see S1 and S2 in Fig. 1) (Qian et al. 2005a,b).

The shape-changing operation in the process of observation will lead to a relative displacement between adjacent nodes in the cable-net. Meanwhile, three vertexes on a rigid panel are fixed with respect to each other. Thus, adaptive connecting mechanisms between panels and the cable-net are certainly needed.

Based on these aforementioned requirements, the present work focuses on the following aspects. Firstly, the degrees of freedom of adaptive connecting mechanisms were designed so that we can not only adapt the panels to match the deformed shape of the cable-net, but

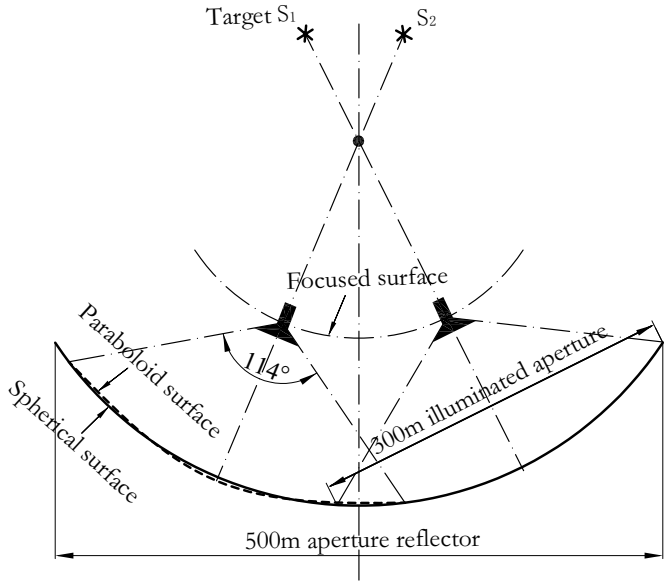

Fig. 1 Geometric optical principle of FAST.

also restrict a given panel to its right place. Secondly, finite element and theoretical analyses were applied to calculate the scope of motion for the adaptive connecting mechanisms during the cable-net's shape-changing operation, and thus provide input parameters for the design size of the adaptive connecting mechanisms. In addition, the gap size between the panels is also investigated to solve the trade-off between avoiding collisions among panels and increasing the observation efficiency of FAST.

2 DESIGN OF THE ADAPTIVE CONNECTING MECHANISM

Three nodes on each panel are connected to the cable-net through adaptive connecting mechanisms. Over-constraint causes adverse effects, since the surface precision of the panel may be influenced by additional stress, while under-constraint may lead to a panel not being restricted to its right place. Thus we should allow the degrees of freedom for each panel to be exactly six. The design for the degrees of freedom is shown in Figure 2.

It can be readily seen that the rotational degrees of freedom are completely released from the three connecting mechanisms. Adaptive connecting mechanism 0 constrains the three translational degrees of freedom ($U_x = U_y = U_z = 0$), adaptive connecting mechanism 1 releases translational degrees of freedom along the axis of the connecting rod ($U_y = U_z = 0$), and adaptive connecting mechanism 2 releases two translational degrees of freedom in the plane of the panel ($U_z = 0$). Under this constraint condition, a panel can not only be fixed well on the nodes of the cable-net, but also adapts itself well to the deformation of the cable-net.

Detailed structures of adaptive connecting mechanisms 0, 1 and 2 are designed according to the aforementioned principles as shown in Figure 3. Adaptive connecting mechanisms 0 and 1 use the scheme of a centripetal joint bearing with a stainless steel rod, and adaptive connecting mechanism 2 uses the scheme of the ball axis with a plane sliding side. Such designs ensure the mechanisms run smoothly in the planned directions, and have the advantages of corrosion-resistance and easy maintenance.

The cable-net structure is formed by the geodesic mesh, and comprises approximately 2225 cross nodes and 4450 panels. Six connecting mechanisms are required on each node according to the geometric topology of the structure. From the results of comparing different schemes, the pattern of arrangement for connecting mechanisms 0, 1 and 2 is adopted, as shown in Figure 4.

The arrangement shown in Figure 4 has two advantages. First, the adaptive connecting mechanisms have the same arrangement on all nodes, which reduces the possibility of installation errors. Second, the arrangement avoids two type 2 mechanisms from being arranged in an adjacent position, which minimizes the possibility of mutual interference during the operation of FAST.

According to the above arrangement, six connecting mechanisms are arranged on each cross node, and a disk-

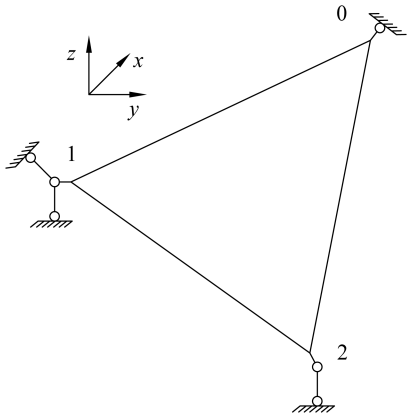

Fig. 2 Degrees of freedom for the adaptive connecting mechanisms.

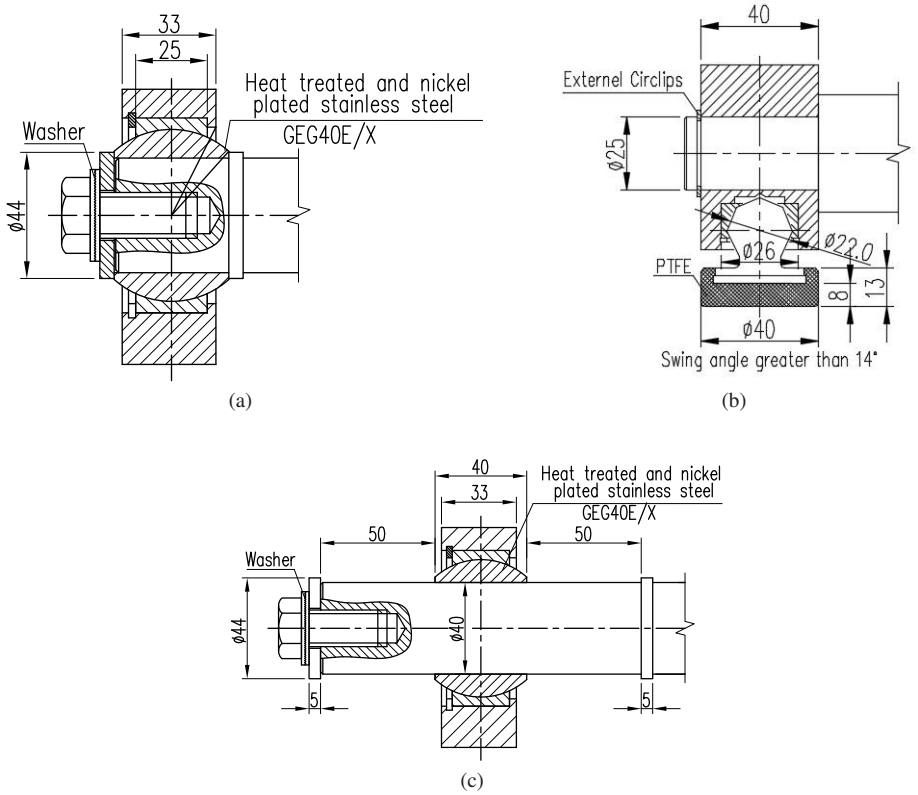

Fig. 3 Sketches of adaptive connecting mechanisms 0 (a), 2 (b) and 1 (c).

type node for positioning the adaptive connecting mechanisms is connected to a cross node through a rigid steel column, as shown in Figure 5.

3 ANALYSIS METHOD

A finite element model describing the reflector system is established using ANSYS software. The disk-type node is simulated by the BEAM44 element, and adaptive connecting mechanisms 0, 1 and 2 are simulated by releasing the corresponding degrees of freedom at the end of the beam. The reflector panel and its back frame are simulated by the SHELL63 element. According to the principle of equal stiffness, the cross nodes are also simulated by the BEAM44 element, and the six beam elements are connected by rigid joints. The cross nodes and disk-type nodes are connected by rigid joints, as shown in Figure 6.

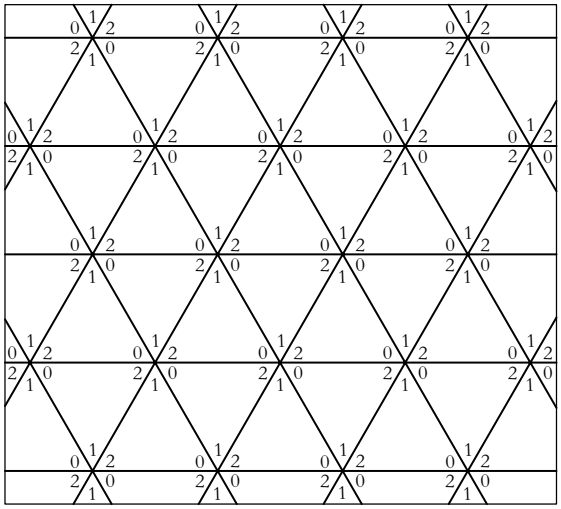

Fig. 4 Arrangement of the adaptive connecting mechanisms.

The initial gap between adjacent panels is set as 100 mm, and the corresponding adjacent edges of panels are parallel to each other. The ring beam structure is modeled using the BEAM4 element. The complete finite element model is shown in Figure 7.

To ensure the correctness of the finite element analysis (FEA), a theoretical algorithm is used to verify the results calculated by FEA.

Figure 8 is a sketch of a single panel. In the sketch, point M represents the panel's vertex near adaptive connecting mechanism 0, and point m represents the connection point of the adaptive connecting mechanism with the panel. Points M' and m' respectively represent the corresponding points on the panel after deformation. Similarly, Points N and P respectively represent the panel's vertices near adaptive connecting mechanisms 1 and 2, and n and p represent the corresponding connection points of the adaptive connecting mechanism and panel. Additionally, N', n', P' and p' represent corresponding points on the panel after deformation.

In theory, if the displacement of the support is previously known, according to the geometric relations and boundary constraints, accurate positions of the adaptive connecting mechanisms after deformation can be obtained by the theoretical algorithm.

To simplify the process of finding a solution, we ignore insignificant factors and apply the following assumptions: (1) the triangular panel is rigid and does not undergo elastic deformation; (2) the angular displacement of the cross node can be neglected and the displacement of the supporting point of the mechanism is equal to that of the cross node; (3) before and after deformation, adaptive connecting mechanisms 0 and 1 are respectively located at the angle bisectors of $\angle NMP$ and $\angle MNP$.

According to the above assumptions and combined with constraints on the adaptive connecting mechanisms, we establish a set of equations with which to obtain the coordinates of points m', n' and p', as shown below.

The coordinates of m' are obtained by Equation (1)

$$\begin{cases} (x_{m'}-x_{M'})^2+(y_{m'}-y_{M'})^2+(z_{m'}-z_{M'})^2 \\ \qquad =L_{Mm}^2, \\ \frac{x_{m'}-x_{M'}}{a_{M'm'}}=t_{m'}, \\ \frac{y_{m'}-y_{M'}}{b_{M'm'}}=t_{m'}, \\ \frac{z_{m'}-z_{M'}}{c_{M'm'}}=t_{m'}. \end{cases} \tag{1}$$

The coordinates of n' are obtained by Equation (2)

$$\begin{cases} (x_{n'}-x_{m'})^2+(y_{n'}-y_{m'})^2+(z_{n'}-z_{m'})^2 \\ \qquad =L_{mn}^2, \\ \frac{x_{n'}-x_{N'}}{a_{N'n'}}=t_{n'}, \\ \frac{y_{n'}-y_{N'}}{b_{N'n'}}=t_{n'}, \\ \frac{z_{n'}-z_{N'}}{c_{N'n'}}=t_{n'}. \end{cases} \tag{2}$$

The coordinates of p' are obtained by Equation (3)

$$\begin{cases} ax_{p'}+by_{p'}+cz_{p'}=1, \\ (x_{p'}-x_{m'})^2+(y_{p'}-y_{m'})^2+z_{p'}-z_{m'})^2=L_{mp}^2, \\ (x_{p'}-x_{n'})^2+(y_{p'}-y_{n'})^2+(z_{p'}-z_{n'})^2=L_{np}^2. \end{cases} \tag{3}$$

The direction of the vector $\boldsymbol{M'm'}$ ($a_{M'm'}$, $b_{M'm'}$, $c_{M'm'}$) is consistent with the angle bisector $\angle N'M'P'$. It can be obtained by Equation (4) that

$$M'm'=\frac{M'N'}{|M'N'|}+\frac{M'P'}{|M'P'|}. \tag{4}$$

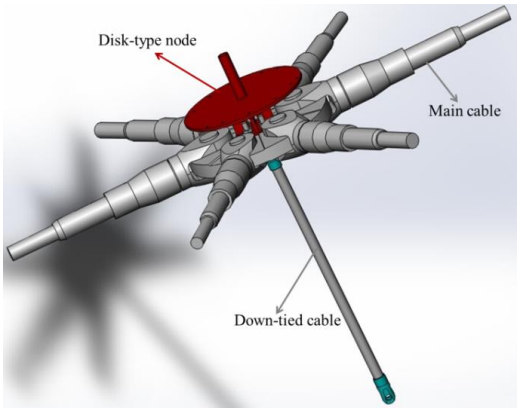

(a) Sketch of the disk-type node.

(b) Arrangement of six connecting mechanisms on the disk-type node.

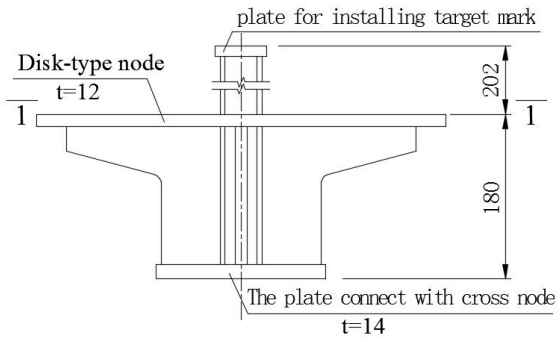

(c) Section view drawing of the disk-type node.

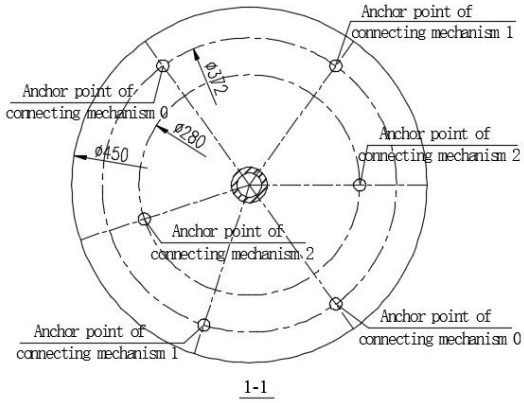

(d) Section view drawing of the disk-type node.

Fig. 5 Sketch of the disk-type node and the arrangement of connecting mechanisms.

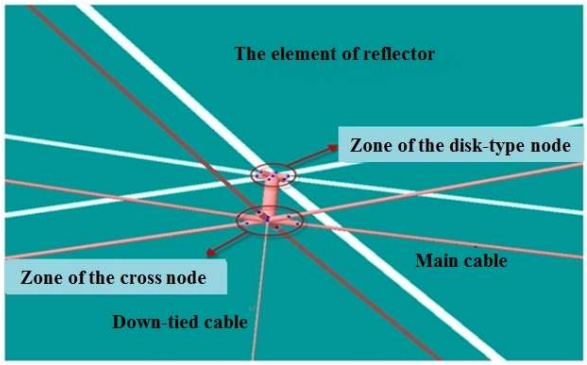

Fig. 6 Finite element model of the reflector unit and main cable connection.

The direction of the vector $\boldsymbol{N'n'}$ ($a_{N'n'}$, $b_{N'n'}$, $c_{N'n'}$) is consistent with the angle bisector $\angle M'N'P'$. It can be obtained by Equation (5) that

$$M'n' = \frac{N'M'}{|N'M'|} + \frac{N'P'}{|N'P'|}, \tag{5}$$

where a, b and c are the three real constants of the plane equation. Based on coordinates of points M', N' and P' that we have considered, its value can be obtained by

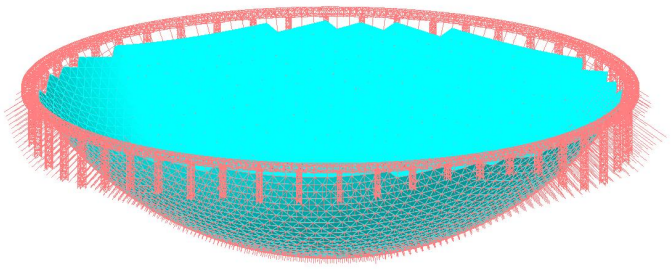

Fig. 7 Finite element model of the FAST reflector system.

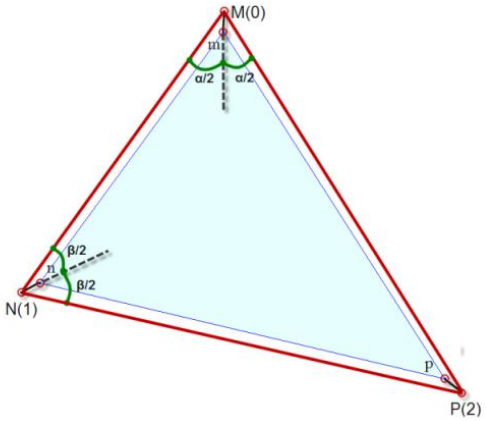

Fig. 8 Sketch of nodes and geometric relationship.

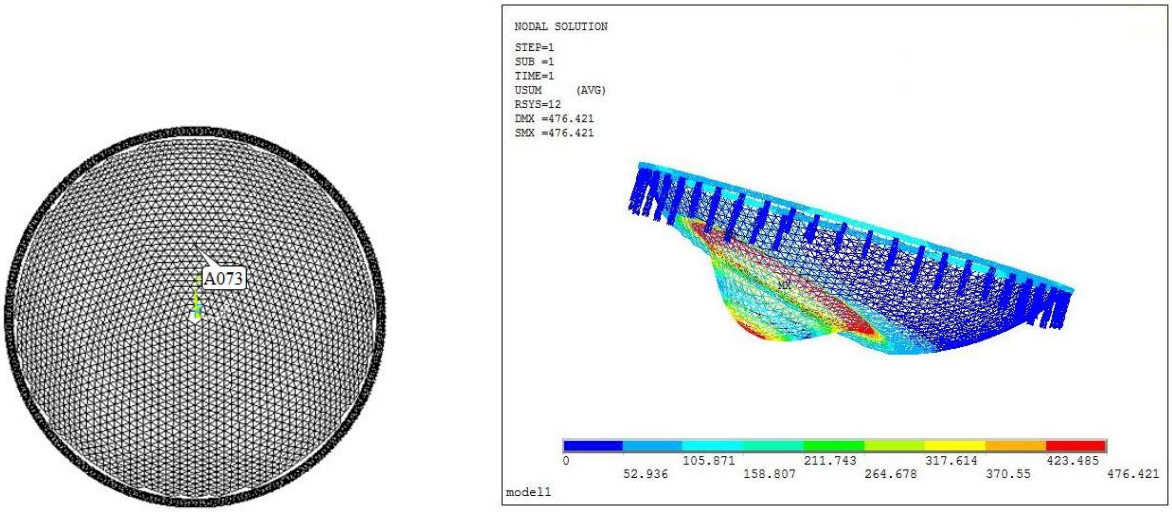

Fig. 9 Location of point A073 and the deformation cloud calculated by FEA.

Equation (6)

$$\begin{cases} ax_{M'} + by_{M'} + cz_{M'} = 1, \\ ax_{N'} + by_{N'} + cz_{N'} = 1, \\ ax_{P'} + by_{P'} + cz_{P'} = 1. \end{cases} \quad (6)$$

According to the geometric relations before and after the deformation, we can also derive the following equations:

$$(x_M - x_m)^2 + (y_M - y_m)^2 + (z_M - z_m)^2 = L_{Mm}^2. \quad (7)$$

$$(x_n - x_m)^2 + (y_n - y_m)^2 + (z_n - z_m)^2 = L_{mn}^2. \quad (8)$$

$$(x_p - x_m)^2 + (y_p - y_m)^2 + (z_p - z_m)^2 = L_{mp}^2. \quad (9)$$

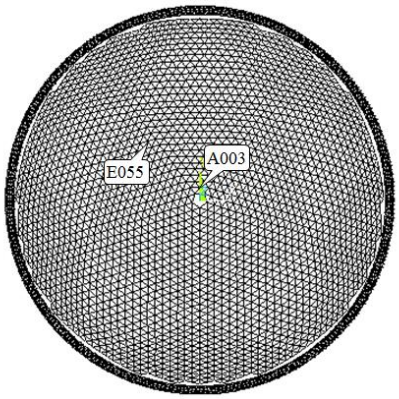

Fig. 10 Positions of points A003 and E055.

$$(x_p - x_n)^2 + (y_p - y_n)^2 + (z_p - z_n)^2 = L_{np}^2. \quad (10)$$

Based on the nodal coordinates of the cross nodes before and after deformation, and the nodal coordinates of the adaptive connecting mechanisms before deformation, we can obtain the value of the following parameters: $a_{M'm'}$, $b_{M'm'}$, $c_{M'm'}$, $a_{N'n'}$, $b_{N'n'}$, $c_{N'n'}$, a, b, c, L_{Mm}, L_{mn}, L_{mp} and L_{np}, by Equations (4) $\sim$ (10). Thus, the unknowns of Equations (1) $\sim$ (3) are simply the coordinates of m', n' and p', and the parameters $t_{m'}$ and $t_{n'}$. They can be solved by the 11 expressions of Equations (1) $\sim$ (3). Taking into account the parameters involved in the above equation and the complexity of the constraint conditions, t_n, MATLAB is used to compute the solution.

A073 is selected as the center of the parabolic shape. The description and analysis method used in simulating the shape-changing operation can be found in literature (Jiang et al. 2015). According to the coordinates of the cross nodes before and after deformation, we can obtain the nodal coordinates of all adaptive connecting mechanisms after deformation using the theoretical algorithm, and then compare the results of the theoretical algorithm with results of FEA (location of point A073 and the deformation cloud calculated by FEA are shown in Figure 9).

Table 1 lists the maximum position deviation of all three types of adaptive connecting mechanism nodes obtained using these two calculation methods.

It can be seen from Table 1 that the maximum deviation of the results derived by these two methods is 3.9 mm. There are a total of 171 nodes for which position deviation is larger than 2 mm in terms of statistics. It is found that these nodes are mainly distributed on the edge of the parabolic surface. In this area, the position of the reflector shows relatively large deviations compared to the normal shape. Thus, the deflection angle of the disk-type node attached to the main cable in this area is relatively large, which leads to an error in the results obtained using the theoretical algorithm. Overall, the results obtained using the two methods are in good accordance, thus showing that the finite element model established in this paper can simulate the actual working condition with good accuracy. Considering that the method used by ANSYS can be developed into an automated program with ANSYS Parametric Design Language (APDL), we will study the adaptive connecting mechanisms through the FEA method.

4 ANALYSES OF THE SCOPE OF MOTION FOR ADAPTIVE CONNECTING MECHANISMS

In the analysis of the FAST cable-net, the shape-changing operation of the FAST cable-net can be simplified as a quasi-static process here. Since the parabolic deformation area cannot exceed a 500 m edge and the illumination aperture is 300 m, the region of motion for the center of the parabolic reflector is restricted to within 26.4°. This region contains 550 cross nodes. We assume that the distribution of the 550 discrete points is sufficiently dense, and that any possible observation state is approximately equivalent to one of the 550 deformation states whose illuminated aperture centers correspond to these 550 cross nodes (Jiang et al. 2013; Jiang et al. 2015; Kong et al. 2013).

According to FEA of the 550 deformation states, the displacements of the six adaptive connecting mechanisms on all disk-type nodes are calculated under the deformation states. Limited by space, in this paper we only show the results of two connecting mechanisms (having locations displayed in Figure 10) with relatively large displacements in terms of type as displayed by the scatter diagrams of displacement distribution in Figure 11.

Figure 11 shows that the distribution range of adaptive connecting mechanism 1 is linear, with extensions (in the coordinate direction) and adductions less than 30 mm. The distribution range of adaptive connecting mechanism 2 is basically elliptical, with extensions (in coordinate direction) and adductions also less than 30 mm, and tangential direction (perpendicular to the extending direction) space less than 50 mm.

Because all adaptive connecting mechanisms are placed on a circular disk-type node, the outer diameter of the disk-type node and the structural size of the adaptive connecting mechanism determine the scope of motion for the adaptive connecting mechanism.

Table 1 Maximum Position Deviation of Adaptive Connecting Mechanism Nodes

Type of connecting mechanism	Maximum position deviation (mm)		
	dx	dy	dz
Adaptive connecting mechanism 0	1.36	1.18	1.68
Adaptive connecting mechanism 1	2.55	1.16	1.02
Adaptive connecting mechanism 2	3.90	2.90	1.60

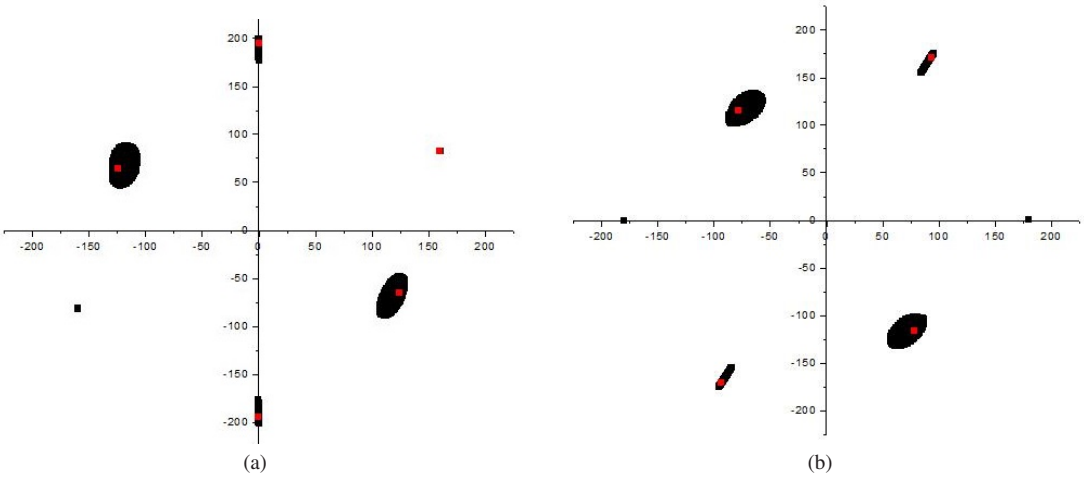

Fig. 11 Scatter diagram showing the displacement distributions of connecting mechanisms at points A003 (a) and E055 (b).

Because the arrangement of adaptive connecting mechanism 1 adjacent to connecting mechanism 2 with an angle of 54° is the arrangement in which mechanisms are most likely to interfere with each other, we study the actual scope of motion of the adaptive connecting mechanisms in this situation. Assuming that the diameter of the disk-type node is 450 mm, and considering the design size of the adaptive connecting mechanism (see Fig. 3), the maximum scope of motion for connecting mechanisms 1 and 2 can be obtained, as traced by dashed lines in Figure 12.

It can be seen from Figure 12 that if the diameter of the disk-type node is 450 mm, the scope of motion for adaptive connecting mechanism 1 should be as follows: extension 50 mm and adduction 60 mm. The scope of motion for connecting mechanism 2 should be as follows: extension 30 mm, adduction 35 mm and tangential range $\pm$50 mm.

The FEA results listed above show that using the disk-type node with a diameter of 450 mm can basically avoid the situation of adaptive connecting mechanisms interfering with each other. However, as the above analysis does not consider the effect of rotation for a disk-type node, a disk-type node is recommended with a diameter of 500 mm in actual construction.

5 RESEARCHES ON THE GAP SIZE BETWEEN PANELS

The accuracy of the surface shape defined by the reflectors directly determines the observation efficiency of FAST. Large gaps between panels will increase the noise level of the received signal. According to calculations done by professionals associated with FAST, every 1 cm growth in the width of gaps between panels is accompanied by a 0.5 K increase in the system noise which is caused by thermal noise from the ground. However, too small a gap may lead to collisions between panels under certain observation conditions. Thus, it is advantageous to determine a reasonable size for the gap between panels to optimize the observation efficiency of FAST.

We use mathematical methods to solve this problem through the finite element method. A sketch of the region representing a gap between panels is shown in Figure 13.

In Figure 13, points I and J represent cross nodes, points A, B, C and D represent the connection points of the adaptive connecting mechanisms with the panels, and φ and θ respectively represent the angle between the two lines IA and IB and the angle between the two lines JC and JD. If there is a collision between panels E1 and E2, then line AC must intersect line BD at some point.

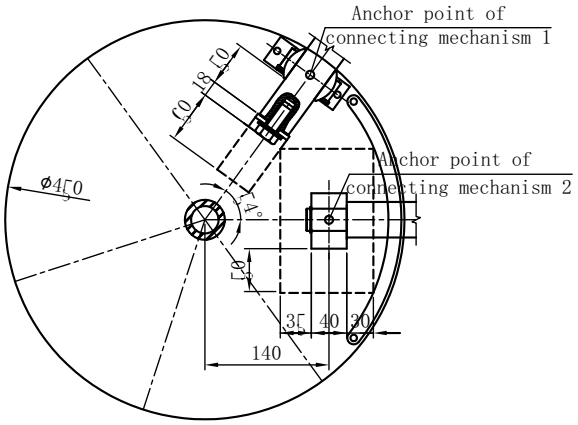

Fig. 12 Adaptive connecting mechanisms 1 and 2 in an adjacent arrangement.

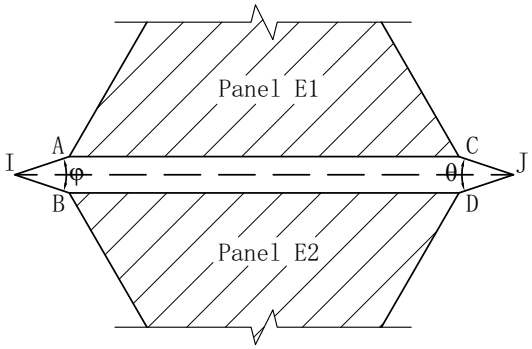

Fig. 13 Sketch of the region representing a gap between panels.

Table 2 Panel Collision Detection Data

Change of temperature	Maximum value of direction change for normal vector	Minimum gap between panels after deformation (mm)	Maximum gap between panels after deformation (mm)
0°	2.2°	58.7	141.0
+25°	2.4°	55.7	142.7
–25°	2.4°	61.0	139.8

According to the vector geometry, we obtain the normal vector of the plane **IAB** from the cross-product of vector ***IA*** and vector ***IB***, which is denoted $\boldsymbol{F}_{\mathbf{IAB}}$. Similarly, we get the normal vector of the plane **JCD** from the cross-product of vector ***JC*** and vector ***JD***, which is denoted $\boldsymbol{F}_{\mathbf{JCD}}$. Obviously, if there is a collision between panels E1 and E2 under a certain observation condition, the change in the direction of normal vector $\boldsymbol{F}_{\mathbf{IAB}}$ or $\boldsymbol{F}_{\mathbf{JCD}}$ must be larger than 90°. We thus judge whether a collision has occurred by observing changes in direction of normal vectors $\boldsymbol{F}_{\mathbf{IAB}}$ or $\boldsymbol{F}_{\mathbf{JCD}}$.

The problem of collisions among FAST panels under a certain gap condition is analyzed using the above principles of collision detection. The initial gap between adjacent panels is set to 100 mm, and the linear expansion coefficient of panels is $1.2\times10^{-5}\,\mathrm{m}\,^{\circ}\mathrm{C}^{-1}$, assuming the temperature change of the panels is within the range 25 °C. According to the FEA of 550 deformation states, a change in the direction of normal vector $\boldsymbol{F}_{\mathbf{IAB}}$ or $\boldsymbol{F}_{\mathbf{JCD}}$ and the gaps between adjacent panels after deformation are calculated. Extreme values of the results are given in Table 2.

It can be seen from Table 2 that the maximum value of a direction change for the normal vector is 2.4° for all 550 deformation states. The panels will therefore not collide with each other under the above conditions. Moreover, Table 2 shows that the minimum gap and maximum gap between adjacent panels are respectively 55.7

and 142.7 mm under the above conditions, and the relative displacement of the panel is not more than 45 mm. Obviously, the initial gap is large enough to avoid a collision. Taking production errors into account, it is recommended to use a gap of 65 mm between panels in actual construction.

6 CONCLUSIONS

In this paper, based on theoretical verifications, an overall finite element model of FAST is established, which consists of adaptive connecting mechanisms. The following contributions were made according to the analysis of finite element computing results.

(1) The present work rationally designed the degrees of freedom of adaptive connecting mechanisms, such that the panels can be reasonably restricted. Moreover, additional stress caused by movement of the cable-net is also avoided, and accuracy of the panels is ensured.
(2) The topological layouts of adaptive connecting mechanisms were designed. Three types of adaptive connecting mechanisms were arranged in the same way on each node, which benefits management of the production of large quantities of components.
(3) The scope of motion for the adaptive connecting mechanisms of FAST was studied, and parameters were thus obtained for design of the size of a disk-type node.
(4) Results of analysis suggest using a disk-type node with a diameter of 500 mm for FAST.
(5) The size of the gap between panels was investigated to solve the trade-off between avoiding panel collision and increasing observation efficiency of FAST. A suitable gap between panels was determined.

Acknowledgements This work was supported by the National Natural Science Foundation of China (Grant Nos. 11303059 and 11673039), the Chinese Academy of Sciences Youth Innovation Promotion Association, CAS Key Technology Talent Program and the FAST FELLOWSHIP. The FAST FELLOWSHIP is supported by Special Funding for Advanced Users, budgeted and administrated by the Center for Astronomical Mega-Science, Chinese Academy of Sciences (CAMS). We would like to thank all our colleagues for their contributions to our study.

References

Jiang, P., Wang, Q. M., & Zhao, Q. 2013, Engineering Mechanics, 30, 400
Jiang, P., Nan, R.-D., Qian, L., & Yue, Y.-L. 2015, RAA (Research in Astronomy and Astrophysics), 15, 1758
Kong, X., Jiang, P., & Wang, Q. M. 2013, Engineering Mechanics, 30S, 169
Li, G., Shen, L., Luo, Y., Deng, C., & He, Y. 2001, Astrophysics and Space Science, 278, 225
Lu, Y., & Ren, G. 2007, Engineering Mechanics, 24, 165
Luo, Y.-F., Deng, C.-G., Li, G.-Q., & Qiu, Y.-H. 2000, Journal-Tongji University, 28, 497
Luo, Y.-F., Yu, Q.-X., Lu, Y., & Li, G.-Q. 2003, Journal-Tongji University, 31, 1
Nan, R., Ren, G., Zhu, W., & Lu, Y. 2003, Acta Astronomica Sinica, 44, 13
Nan, R., Li, D., Jin, C., et al. 2011, International Journal of Modern Physics D, 20, 989
Qian, H., Fan, F., Shen, S., & Wang, Q. 2005a, Journal of Harbin Institute of Technology, 37, 750
Qian, H., Fan, F., Shen, S., et al. 2005b, China Civil Engineering Journal, 38, 18
Ren, G.-X., Lu, Q.-H., & Zhou, Z. 2001, Astrophysics and Space Science, 278, 243